Eliott	Guenat	Eliott.guenat@epfl.ch
First	*Last*	*E-mail*

Paper title Performance potential of gas foil thrust bearings enhanced with spiral grooves

Authors: Guenat, Eliott ; Schiffmann, Jürg

Elsevier journal Tribology International

Transactions: Volume 131, Pages 438-445

Date of Publication: 12.11.2018

DOI: https://doi.org/10.1016/j.triboint.2018.11.003

Science direct https://www.sciencedirect.com/science/article/pii/S0301679X18305437?via%3Dihub

Performance Potential of Gas Foil Thrust Bearings Enhanced with Spiral Grooves

Eliott Guenat[1], Jürg Schiffmann

Ecole Polytechnique Fédérale de Lausanne, Laboratory for applied mechanical design, Maladière 71b, CP 526, CH-2002 Neuchâtel 2

Abstract

The upscaling of turbomachinery using gas foil thrust bearings is limited because of their limited load capacity and the thermal issues linked with very thin film thickness. The improvement potential of spiral grooves manufactured on the top-foil of such bearings is investigated in terms of load capacity and drag torque for a wide range of ramp depth, compressibility number and bearing compliance. Multi-objective optimization of grooves parameters allows to identify a trade-off between the drag reduction and the load capacity improvement. In some cases, load capacity improvements reach nearly 70% or drag torque at equal load diminishes by 40%. However, the results suggest that the ultimate load capacity of the bearing is reduced compared to plain gas foil thrust bearings.

Keywords: Gas Lubrication, Foil Bearings, Axial thrust bearing, Simulation

[1]Corresponding author. Email adress: eliott.guenat@epfl.ch

Roman symbols

a	Groove length (m)
b	Ridge length (m)
c_s	NGT coefficient (-)
e	Eccentricity (m)
f	NGT coefficient (-)
g	NGT coefficient (-)
h	Clearance (m)
h_0	Nominal clearance (m)
h_g	Groove clearance (m)
h_r	Ridge clearance (m)
h_R	Ramp depth (m)
K	Foil stiffness (Nm^{-3})
P	Pressure (Pa)
R	Radius (m)
r	Radial coordinate (m)
s	Bump foil pitch (m)
T	Drag torque (Nm)
T_r	Drag torque ratio (-)
W	Load capacity (N)
W_r	Load capacity ratio (-)

Greek symbols

α	Groove aspect ratio, compliance (-)
$\hat{\beta}$	Groove angle (°)
δ	Groove depth (m)
ϵ	Eccentricity ratio (-)
θ	Circumferential coordinate (-)
Λ	Compressibility number (-)
μ	Dynamic viscosity (Pa s)
ω	Angular velocity (rad s^{-1})

Superscripts

$-$	Non-dimensional

Subscripts

a	Ambient condition
F	Foil
g	Groove
i	Inner
o	Outer
R	Ramp
r	Ridge, ratio

Acronyms

$GFSGTB$	Gas foil spiral groove thrust bearing
$GFTB$	Gas foil thrust bearing
NGT	Narrow groove theory
$SGTB$	Spiral groove thrust bearing

1. Introduction

Gas Foil Thrust Bearings (GFTB) are widely used in oil-free airborne applications such as microturbomachinery. While the first applications of this technology were small-scale with modest loads, global research efforts are being made toward the application of the compliant gas bearing technology to upscaled systems, with larger loads, in order to broader the scope of application of GFTB and oil-free bearings in general.

1.1. Nature of the issue

Heshmat [1] proposed a model of GFTB considering the compliant bump foil as a simple elastic foundation and performed a parametric study to identify the geometry maximizing the load capacity. A considerable effort was spent by the community on the refinement of this model, implementing more complex foundation models or refining the method for the computation of the compliance coefficient. The layout of GFTB studied by Heshmat is a widely used design in oil-free turbomachinery applications such as supercritical CO_2 compressors [2] or turbochargers [3]. Moreover, the model developed decades ago by Heshmat is still of use in the recent literature, showing a reasonable agreement with experimental data [2, 3, 4]. The upscaling trend in size of rotors supported on foil bearings is limited by their load capacity and drag losses, which may lead to a delicate thermal management [5]. Scaling laws do not play in favor of larger applications, as showed by Prasad [6] and Dellacorte [7]. To overcome this intrinsic limitation, researchers have investigated numerous possibilities to further increase the load capacity of GFTB. The clearance distribution was optimized by Lehn [8] to maximize the load capacity using a gradient-based optimization. A hybrid foil thrust bearings was investigated by Lee et Kim [9], where compressed air is supplied to the bearing fluid film in order to sustain a thin lubricating gas film even at high load. Magnetic bearings can also be a solution to relieve the aerodynamic bearing, as suggested by Heshmat et al. [10]. Both alternatives imply the use of auxiliaries, which is costly in terms of space, investment and power and reduces the reliability.

In the meantime, the development of rigid spiral groove thrust bearings (SGTB) followed a parallel path, starting with Malanoski and Pan [11] who applied the Narrow Groove Theory (NGT) to model grooved thrust bearings. However, this technology is limited to very small-scale machines because of the tight manufacturing tolerances required. The recent literature brought an promising improvement potential in terms of static stiffness and dynamic stability for SGB with non-constant groove parameters, with the work of Hashimoto et al. [12] and Schiffmann [13].

Despite the progress accomplished, the two technologies remain isolated one from another. An early attempt to combine the SGTB with a compliant structure was realized by Licht in 1981 [14] with a full bearing based on Malanoski's rigid design. The compliant structure was designed such that the top foil remains parallel to the runner under load in order to preserve the validity of Malanoski's performance predictions. Unfortunately, no model was proposed and the improvement potential was not assessed. Based on this work it is hypothesized that the addition of spiral grooves on a GFTB's top foil can be of practical interest in the quest of enhanced load capacities and eased thermal management. Moreover, the manufacturing of grooves is inexpensive and could even be retrofited on existing GFTBs.

1.2. Goals and objectives

The present work investigates the use of spiral grooves manufactured on the GFTB's top foil to improve the load capacity and/or to reduce the drag losses. The objective are to: (1) develop a model for Gas Foil Sprial Groove Thrust Bearings (GFSGTB), (2) investigate the static performance of such bearings in comparison to their ungrooved equivalent in terms of load capacity and losses and (3) devise design guidelines.

1.3. Scope of the Paper

The GFTB model of Heshmat, including a simple foundation model for the compliant structure, is combined with the modified Reynolds equation of the NGT to model the pumping action of logarithmic grooves manufactured on the top foil of the bearing. Multi-objective optimizations are performed for various geometries (ramp depth) and operating conditions in order to identify trade-offs in terms of load capacity and losses. Compressibility numbers up to 1000 are evaluated. The potential of the new bearing geometry is highlighted, as well as its limitations. Based on these results, a set of design guidelines is suggested to take advantage of the new layout.

2. Theory

The layout under investigation consists in an inward-pumping spiral groove thrust bearing, where grooves are located on the outer diameter (Fig.2). Initially, the section covering the angle θ_R, referred as *ramp*, is converging (Fig.

1) with a depth h_R and a nominal clearance h_0. The Narrow Groove Theory is employed to predict the overall pressure in the grooved region of the bearing, assuming a infinite number of groove-ridge pairs, so the pressure variation over a groove-ridge pair vanishes globally, while varying linearly between a groove and the following ridge locally. This hypothesis is equivalent to a local incompressibility of the lubricant. It allows an efficient and effective modelling of groove patterns without the need of fine grid size to capture the grooves individually. The first use of this theory to analyze SGTB was done by Malanoski and Pan [11]. The analysis was later supported by Zirkelback and San Andres [15] with the finite element method. Only the resulting differential equation, as developed in [16] for an isothermal ideal gas for steady state operation is displayed here:

$$\begin{aligned}&\partial_\theta\left[\bar{P}\left(\frac{1}{\bar{r}}f_1\partial_\theta\bar{P}+f_2\partial_{\bar{z}}\bar{P}\right)\right]+\partial_{\bar{r}}\left[\bar{P}\left(f_2\partial_\theta\bar{P}+f_3\bar{r}\partial_{\bar{r}}\bar{P}\right)\right]\\&+c_s\left(\bar{r}\sin\beta\partial_\theta(f_4\bar{P})-\cos\beta\partial_{\bar{r}}(\bar{r}^2f_4\bar{P})\right)=\Lambda\bar{r}\partial_\theta(f_5\bar{P})\end{aligned}\tag{1}$$

where the geometry is presented in Figures 2 and 1 and functions f_i are summarized in the Appendix. This equations applies to the entire bearing domain, reducing to the normal Reynolds equation in the land region, where $\bar{h}_g=\bar{h}_r=\bar{h}$.

The modeling is based on the work by Heshmat [1] using a simple foundation model for the compliant structure. The non-dimensionalization of the governing equation is performed as follows:

$$\bar{P}=P/P_a\quad\bar{r}=r/R_o\quad\bar{h}_{r/g}=h_{r/g}/h_0\quad\Lambda=\frac{6\mu\omega R_o^2}{P_ah_0^2}\tag{2}$$

The non-dimensional ridge and groove clearances are expressed as a function of the position and local pressure :

$$\begin{aligned}\bar{h}_r&=1-\epsilon+g(\theta)+\alpha_F(\bar{P}-1)\\\bar{h}_g&=\bar{h}_r+\bar{\delta}\end{aligned}\tag{3}$$

where the compliance α_F is expressed as follows:

$$\alpha_F=\frac{P_as}{K_fh_0}\tag{4}$$

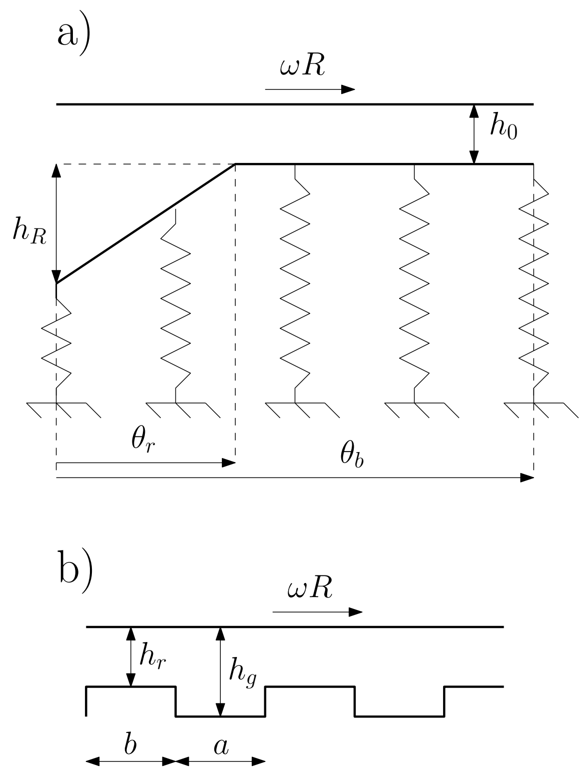

Figure 1: Geometry and nomenclature of GFSGTB

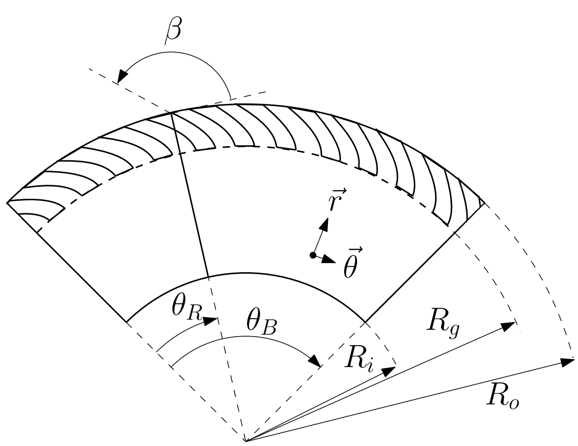

Figure 2: Geometry and nomenclature of inward-pumping GFSGTB

$g(\theta)$ expresses the change in clearance in the converging sector of the fluid film domain:

$$g(\theta) = \max\left[\bar{h}_R\left(1 - \theta/\theta_R\right), 0\right] \tag{5}$$

The term ϵ is the eccentricity ratio, defined as $\epsilon = e/h_0$, with e being the axial displacement of the rotating smooth disk from its nominal position. The boundary conditions of Eq. 1 are ambient pressure at $\bar{r} = R_i/R_o$, $\bar{r} = 1$, $\theta = 0$, $\theta = \theta_B$. On the line $\bar{r} = R_g/R_o$, the continuity of the radial mass flow rate across the land and grooved region is imposed:

$$\dot{m}_{r,groove} = \dot{m}_{r,land} \quad (\bar{r} = R_g/R_o) \tag{6}$$

which leads to the following expression:

$$c_s f_4 \bar{r}\cos\beta - f_2 \frac{1}{\bar{r}}\partial_\theta \bar{P} - f_3 \partial_{\bar{r}} \bar{P} = -\bar{h}^3 \partial_{\bar{r}} \bar{P} \tag{7}$$

The non-linear modified Reynolds equation is discretized using a finite difference scheme and iteratively solved with a successive approximation method [17]. The field of local clearance (Eq.3) is updated based on the previously computed local pressure. The iterative procedure is stopped when the maximum relative error between two successive pressure fields pass below a convergence threshold of 10^{-4}. After a grid sensitivity analysis was performed on the bearing model, a grid of 100 points in the radial direction and 250 in the circumferential direction was selected, which leads to a satisfying convergence.

Because it limits the wider application of the technology, the static performance is of primary importance in the design of gas thrust bearings. It appears more relevant than the dynamic behavior in a first study. Therefore, the performance metrics compare the investigated grooved and smooth layouts are the non-dimensional load capacity $\overline{W}$ and the non-dimensional drag torque $\overline{T}$:

$$\overline{W} = \int_{Ri/Ro}^{1}\int_{0}^{\theta_B} (\bar{P} - 1)\bar{r}\,\mathrm{d}\theta\,\mathrm{d}\bar{r} \tag{8}$$

$$\overline{T} = \int_{Ri/Ro}^{1}\int_{0}^{\theta_B} \left(\frac{\alpha\bar{h}_g + (1-\alpha)\bar{h}_r}{2}\bar{r}\partial_\theta\bar{P} + \frac{\Lambda}{6}\bar{r}^3\left(\frac{\alpha}{\bar{h}_g} + \frac{1-\alpha}{\bar{h}_r}\right)\right)\mathrm{d}\theta\,\mathrm{d}\bar{r} \tag{9}$$

They are linked to their dimensional counterparts as follows:

$$W = P_a R_o^2 \overline{W} \tag{10}$$

$$T = P_a h_0 R_o^2 \overline{T} \tag{11}$$

It is useful to define the load capacity and drag torque of the grooved design normalized by the plain GFTB:

$$\overline{W}_r = \frac{\overline{W}_{grooved}}{\overline{W}_{plain}} \tag{12}$$

$$\overline{T}_r = \frac{\overline{T}_{grooved}}{\overline{T}_{plain}} \tag{13}$$

The outputs of the implemented model are compared to the results of Heshmat [1] as a sanity check for $\bar{h}_R = 1$, $\alpha = 1$, $\theta_B = 45°$ and $\theta_R/\theta_B = 0.5$, $R_o/R_i = 2$, suggesting a good agreement with the experimentally validated model (Figure 3). The largest realtive deviation between the two models occurs at $\Lambda = 40$ and reaches 1.9%.

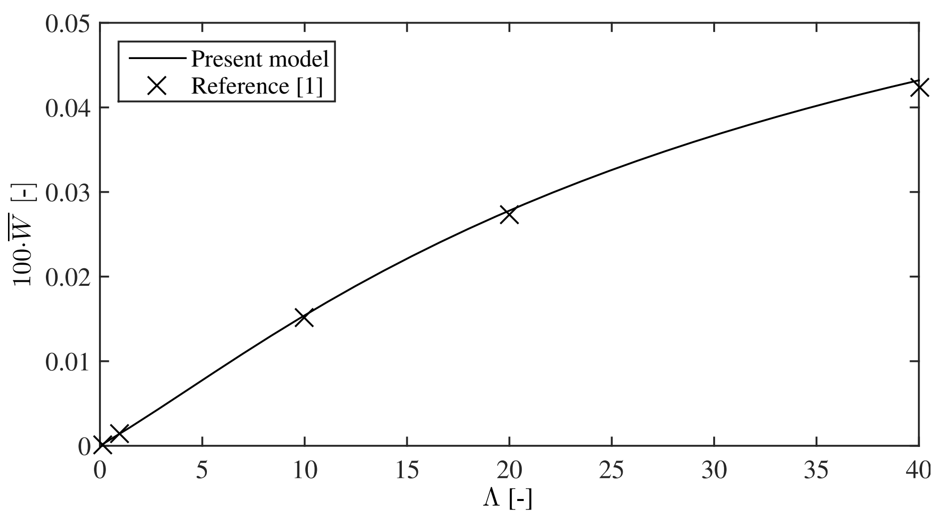

Figure 3: Comparison of the present model with reference [1]

3. Numerical computations and results

The main geometrical parameters of the studied bearings follow the conclusion of Heshmat who identified the layout maximizing the load capacity for GFTB as being $R_o/R_i = 2$, $\theta_B = 45°$ and $\theta_R/\theta_B = 0.5$. The relative ramp height $\bar{h}_R$ is varied from low values ($\bar{h}_R = 1$) to values in the range recommended by Heshmat for maximum load capacity ($\bar{h}_R > 10$). Unless specified differently, the compliance is set to $\alpha_F = 1$ and the eccentricity ratio ϵ to 0.

3.1. Effect of logarithmic grooves on the bearing performance

In order to investigate the effect of grooved top foils on the defined performance indicators and to identify the optimum groove geometries, multi-objective optimizations were performed for different bearing geometries ($\bar{h}_R$) and operating conditions (Λ) simultaneously maximizing the load capacity and minimizing the drag torque. The decision variables are the 4 geometrical parameters describing the grooved region, namely:

$$\bar{h}_g \qquad \in [1, 4] \tag{14}$$

$$\alpha = \frac{a}{a+b} \qquad \in [0.3, 0.7] \tag{15}$$

$$\beta \qquad \in [0, \pi] \tag{16}$$

$$\gamma = \frac{R_g - R_i}{R_o - R_i} \qquad \in [0.1, 0.9] \tag{17}$$

The optimizations were performed using a genetic algorithm [18] with 10^4 evaluations to obtain a satisfying convergence. The outputs of the optimization are Pareto fronts representing the optimal trade-offs between load capacity and drag torque. Am example is given in Figure 4, for the case $\Lambda = 0.1$ and four different values of $\bar{h}_R$. The results clearly suggest the existence of regions with a positive effect of the spiral grooves on the drag torque and on the load capacity compared to plain GFTB. Depending on the constraints of a particular design problem, designers may either choose a solution favoring a high load capacity ratio or a low drag torque ratio. The Pareto fronts obtained for large ranges of h_R and Λ are processed to highlight two metrics of practical interest: (1) the maximum value of $\overline{W}_r$ and (2) the value of $\overline{T}_r$ corresponding to the point where $\overline{W}_r = 1$, which corresponds to (1) maximizing gain in load capacity without considering the drag and (2) minimizing the drag torque without losing load capacity compared to the plain GFTB design, respectively.

Figure 5 represents the maximum $\overline{W}_r$ as a function of the compressibility number for various ramp depth ratios and a constant complaince $\alpha_F = 1$.

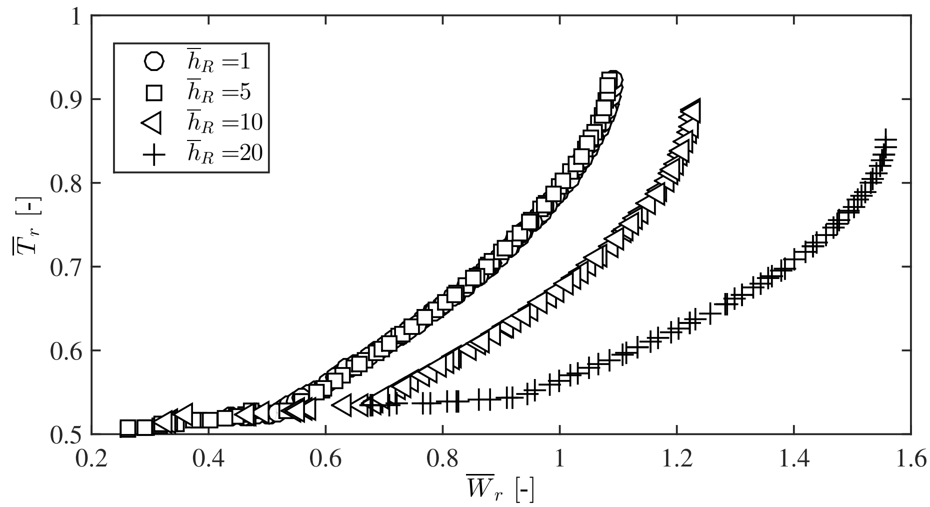

Figure 4: Pareto fronts for $\Lambda = 0.1$ and different ramp depth ratios.

There is a strong influence of the relative ramp depth $\bar{h}_R$ on the potential performance gain. Low values exhibit stronger improvements at high values of Λ and inversely for large $\bar{h}_R$. This behavior can be explained by the absence of a limiting solution for $\Lambda \to \infty$ for rigid grooved bearings modeled with the NGT [19], which limits the performance of the smooth thrust bearings [20]. Ultimately, the results suggest that the maximum $\overline{W}_r$ for grooved thrust bearings is well above 1 for all values of $\bar{h}_R$. Although not captured by the NGT, a limiting solution does exist at very high compressibility in the case of grooved bearings. However, it is shifted to higher compressibility numbers [19], which maintains the interest of using the NGT even at such high values of Λ. For every investigated value of $\bar{h}_R$, a minimum in $\overline{W}_r$ is observed at intermediate values of Λ, where the optimal grooved case is close to the performance of a smooth design. The location of this minimum is shifted toward higher compressibility numbers as $\bar{h}_R$ increases. This is a consequence of the limiting solution at high compressibility numbers: a larger value of $\bar{h}_R$ leads to a limiting solution in pressure rise, which becomes more difficult to overcome by the pumping effect of grooves.

Figure 6 represents the drag loss ratio $\overline{T}_r$ as a function of the compressibility and for various ramp depth ratios at $\overline{W}_r = 1$. The curves show that at equal load capacity, the grooved design can reduce the losses significantly depending on the geometry and the operating conditions. The most promising solutions maximizing the load capacity ratio in Figure 5 are also the most interesting ones regarding the drag reduction in drag torque in Figure 6. In these cases, the whole Pareto front happens to be partially or totally shifted in the domain $\overline{W}_r > 1$, allowing a significant performance in the two metrics. Depending on the case, the reduction of drag torque can exceed 40%. In addition, two optimizations performed at high compressibility numbers (500 and 1000), both with $\bar{h}_R = 1$, only provide Pareto fronts with $\overline{W}_r > 1$. As a consequence, the point of lowest $\overline{W}_r$ (and therefore lowest $\overline{T}_r$) was displayed and the actual value of the load capacity ratio indicated.

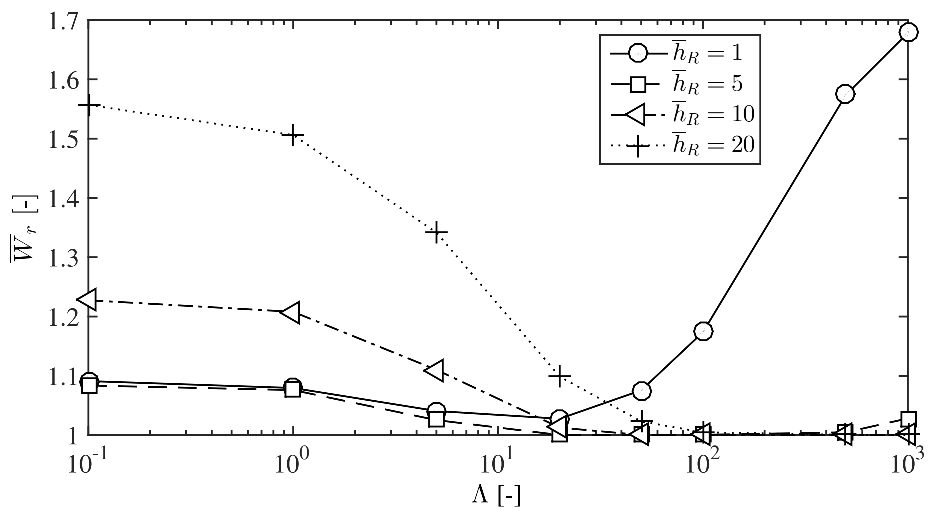

Figure 5: Solutions of maximum $\overline{W}_r$ for a compliance $\alpha_F = 1$

The groove parameters of the solutions for maximum load capacity shown in Figure 5 are displayed in Figure 7. Increasing the value of the ramp depth $\bar{h}_R$ tends to increase the optimum values of $\bar{h}_g$ and α, and decrease β and γ. At very high compressibility numbers Λ, the grooves tend to be deeper and occupy a larger area (higher α and lower γ), in particular for the cases $\bar{h}_R = 1$ and 5. It is important to note that for some cases the optimal design yield $\bar{h}_g = 1$, which corresponds to a plain design, where the other parameter have no influence on the bearing performance, thus explaining their swinging values for these particular cases. The optimal groove geometry does not evolve significantly for $\Lambda < 10$, which is a indicator for good off-design performance, as it will be shown below.

The points corresponding to $\Lambda = 5$ in Figure 5 have their pressure field

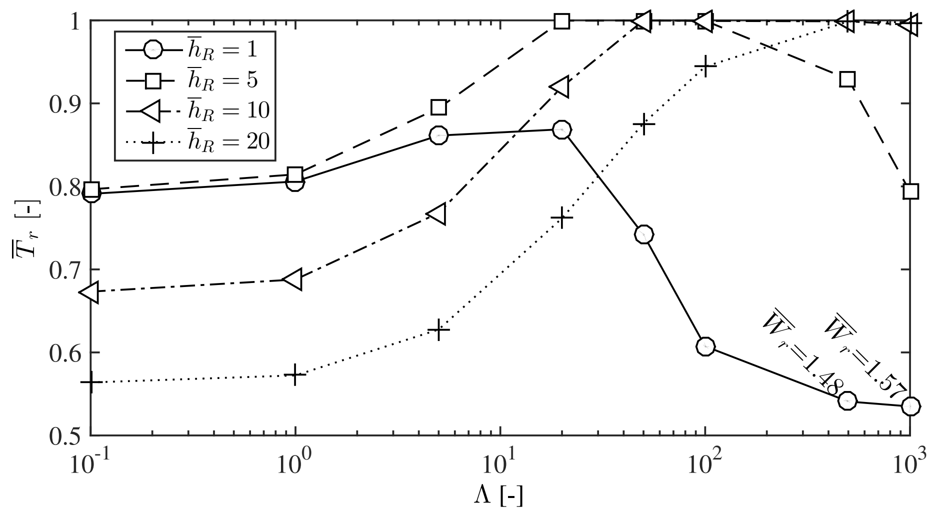

Figure 6: Values of $\overline{T}_r$ for solutions with $\overline{W}_r = 1$ for a compliance $\alpha_F = 1$

represented in Figures 8 and 9. The pressure gradient in t is much stronger along the radial direction in the grooved zone for $\bar{r}_g < \bar{r} < 1$ than in the smooth zone, because of the pumping action of the grooved pattern. As the relative ramp depth increases, the zone of maximum pressure shifts from the center of the bearing toward the plateau, with a zone of maximum pressure bordered by the groove zone. In the ramp zone, the grooves tend to loose their pumping effect and become locally ineffective at building pressure or acting as a radial seal.

Since the presented results correspond to cases with a compliance $\alpha_F = 1$, the influence of this choice on the results is investigated. Figure 10 shows the influence of the foil compliance on the maximum load capacity ratio at a high compressibility number, resulting from an optimization performed at discrete values of α_F. Because of the low pressure build-up in the bearing at low values of Λ, the compliance has little effect on the performance metric because the resulting deflection of the top foil is not significant. $\overline{W}_r$ exhibits a minimum at $\alpha_F \approx 0.35$ and increases approximately linearly at high compliance. However, the relative variation of $\overline{W}_r$ over the considered domain is low. It is therefore suggested that the compliance has little influence on the potential of the GFSTB over the plain GFTB.

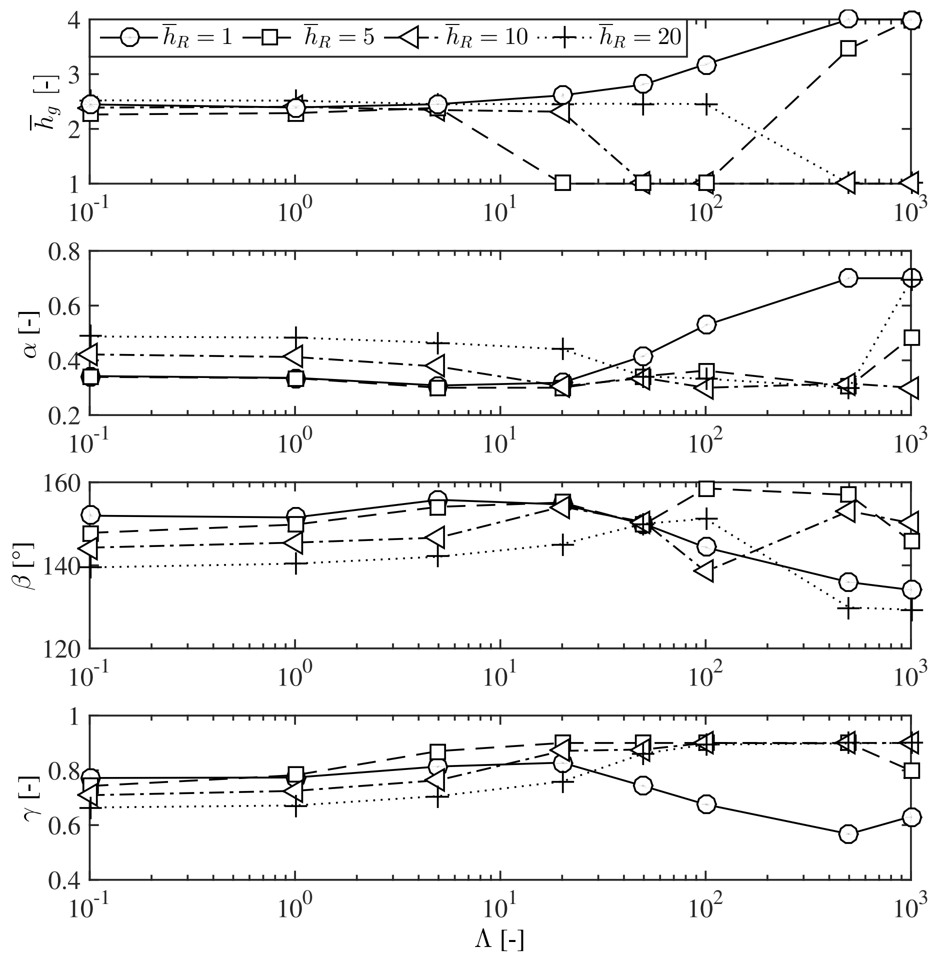

Figure 7: Groove parameters corresponding to solutions in Figure 5

3.2. *Off-design operation*

Figure 11 represents the off-design performance in terms of compressibility number of two geometries with $\bar{h}_R = 20$ maximizing $\overline{W}_r$ at $\Lambda = 0.1$ and 50 respectively, for a compliance $\alpha_F = 1$. Since the optimal groove geometry does not evolve much for the case $\Lambda = 0.1$, the performance remains close to the optimum at low compressibility number, until $\Lambda \approx 20$. $\overline{W}_r$ drops below 1 for higher compressibility numbers. The design optimized for $\Lambda = 50$ maintains its performance close to 1 at high values of Λ with an appreciable gain at low compressibility, although it performs significantly lower than the local optimal geometry.

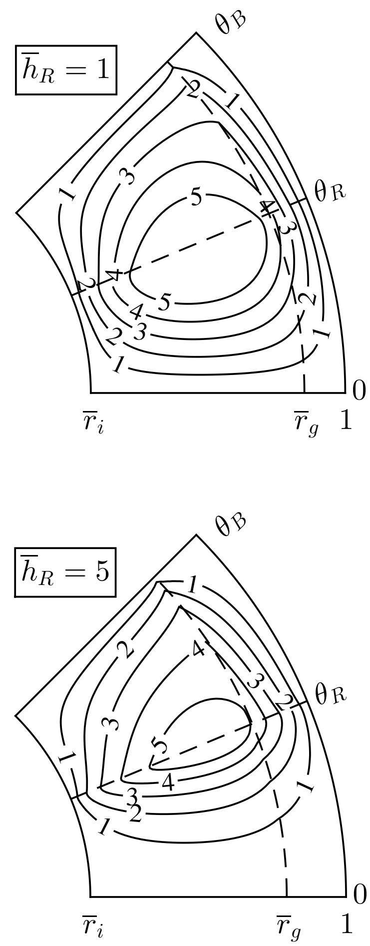

Figure 8: Contour of $100 \cdot (\overline{P} - 1)$ for the geometries maximizing the load capacity at $\Lambda = 5$ and ramp depth $\bar{h}_R = 1$ and 5

Figures 12 and 13 extend this analysis with $\bar{h}_R$ as a second variable, exploring the performance of the geometry optimized for $\Lambda = 0.1$ and $\Lambda = 50$ respectively, with $\bar{h}_R = 20$. The domain of interest with $\overline{W}_r > 1$ is narrowed further in Λ as $\bar{h}_R$ departs from the design value. A local minimum in $\overline{W}_r$ is visible, however with a reduction of less than 15% compared to the design value. The performance increases sharply for low operating $\bar{h}_R$ at

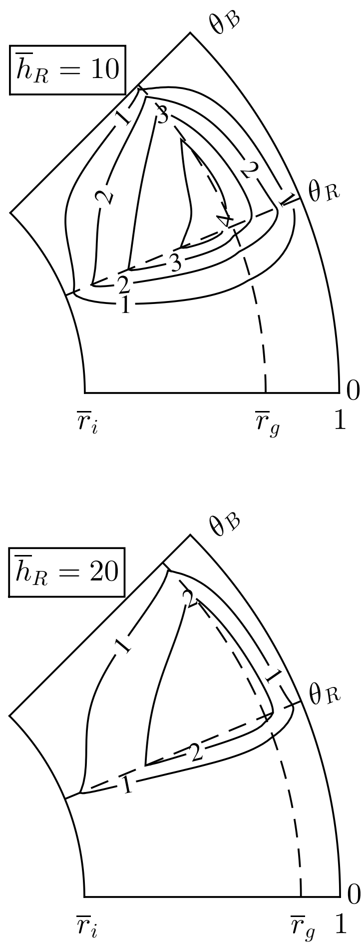

Figure 9: Contour of $100 \cdot (\overline{P} - 1)$ for the geometries maximizing the load capacity at $\Lambda = 5$ and ramp depth $\bar{h}_R = 10$ and 20

high compressibility, which corroborates with the results in Figure 5. It is important to note that for a given off-design value of $\bar{h}_R$, the performance passes through a minimum before increasing again. It supports the mentioned conjecture that an optimal groove design with $\overline{W}_r > 1$ exists at very high values of compressibility number Λ for any value of ramp depth ratio $\bar{h}_R$, as long as the local incompressibility assumption of the NGT is verified

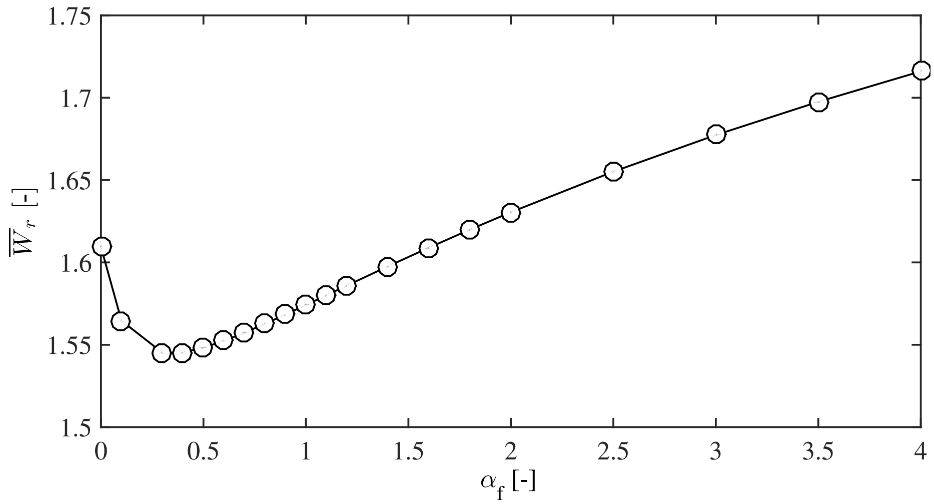

Figure 10: Evolution of the load capacity ratio against the bearing compliance at $\Lambda = 500$ and $\bar{h}_R = 1$

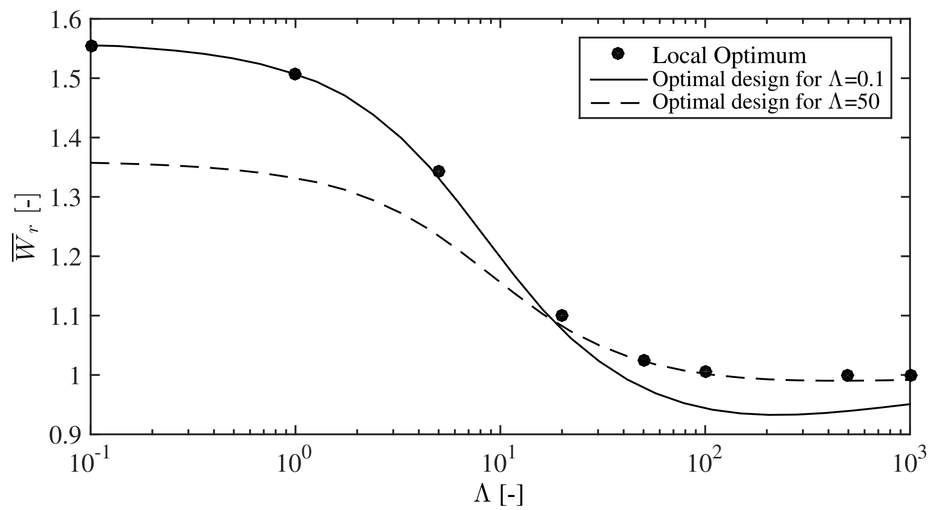

Figure 11: Off-design performance ($\bar{h}_R = 20$) in terms of $\overline{W}_r$ of geometries optimized for $\Lambda = 0.1$ and 50

[19]. A qualitatively similar observation can be made for the performance along the variable $\bar{h}_R$ at constant Λ. In both investigated cases, $\overline{W}_r$ passes through a minimum at $\bar{h}_R \approx 2$ for $\Lambda < 10$. The value of relative ramp height associated with this minimum increases at higher compressibility numbers. Note that cases close to $\bar{h}_R = 0$ represent two parallel surfaces, which are

unable to build-up pressure if grooves are absent. Therefore, $\overline{W}_r$ becomes asymptotically large in these cases.

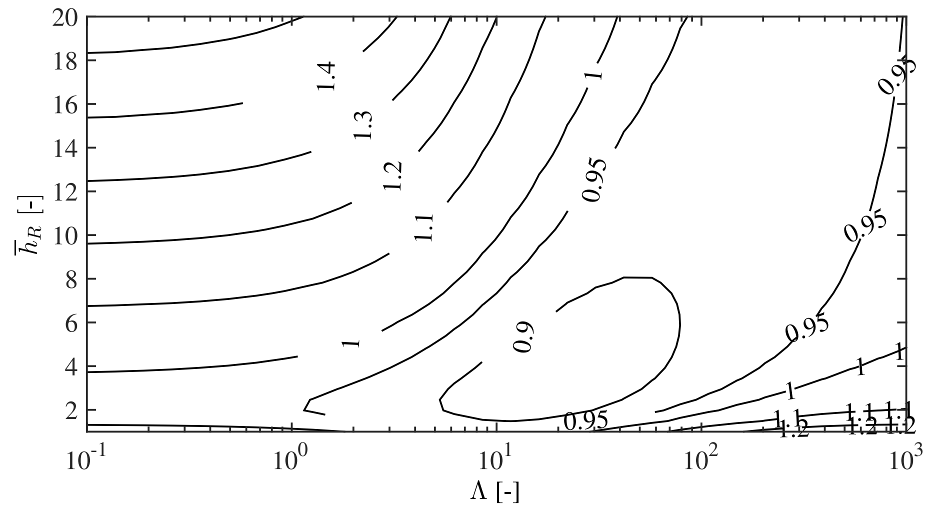

Figure 12: Off-design performance in terms of $\overline{W}_r$ of the geometry optimized for $\Lambda = 0.1$ and $\bar{h}_R = 20$

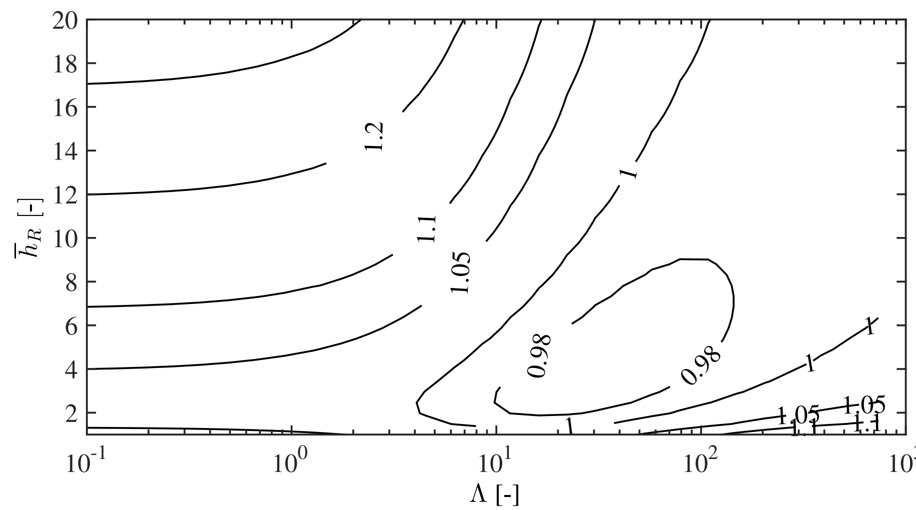

Figure 13: Off-design performance in terms of $\overline{W}_r$ of the geometry optimized for $\Lambda = 50$ and $\bar{h}_R = 20$

The evolution of $\overline{W}_r$ with the eccentricity ratio ϵ is shown in Figure 14. The geometry of the four represented cases maximizes $\overline{W}_r$ at $\epsilon = 0$ and a nominal compliance $\alpha_F = 1$ evaluated at zero eccentricity. Note that for obtaining these results the stiffness of the elastic foundation is kept constant, which, according to Eq.4, leads to a compliance that evolves with eccentricity. All grooved geometries show an improved load capacity in nominal conditions but exhibit a lower performance than the plain GFTB design at high eccentricity ratios, with a loss of nearly 25%. $\overline{W}_r$ reaches a local maximum a high values of $\bar{h}_R$, which is not present for $\bar{h}_R$=1, where it decreases steadily with an increasing eccentricity ratio. Theses results suggest that GFSTB do not provide a higher ultimate load capacity compared to the plain design. They allow though, to achieve higher load capacities at moderate eccentricities, which can be beneficial for the thermal management.

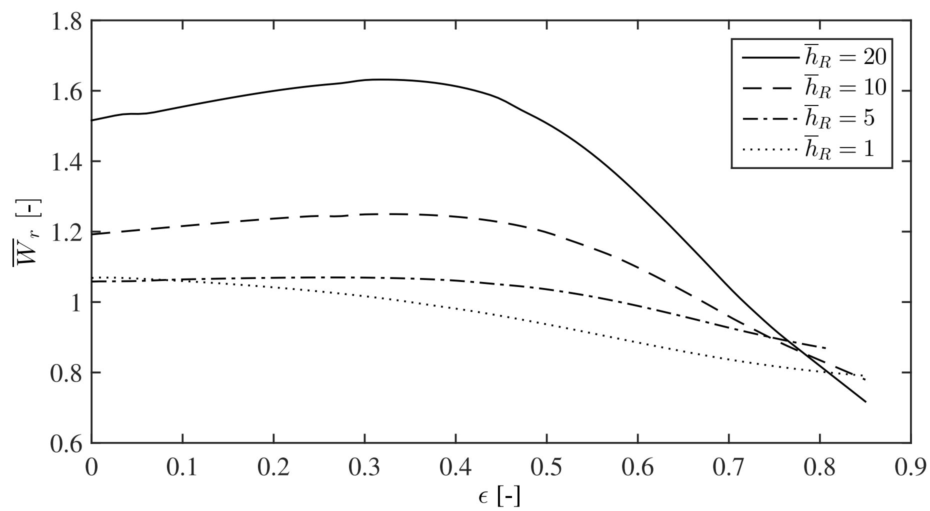

Figure 14: Off-design performance in terms of $\overline{W}_r$ of the geometry optimized for $\Lambda = 1$

4. Conclusions

Based on Heshmat's work [1], a model of gas foil thrust bearing enhanced with logarithmic spiral grooves is developed using the Narrow Groove Theory. The improvement potential is evaluated in terms of load capacity and drag torque for a large range of compressibility numbers, relative ramp depth and bearing compliance. A multi-objective optimization for identifying the optimal groove geometries to maximize the load capacity while minimizing the drag torque leads to the following observations:

- The improvement potential of a grooved bearing compared to a plain one is the highest at low compressibility numbers and large relative ramp depth or inversely at high compressibility numbers and low ramp depths.

- Optimum groove geometries allow to improve the load capacity by nearly 70%.

- Optimum groove geometries allow to decrease the drag torque (losses) of the thrust bearing by up to 40% compared to a plain Gas Foil Thrust Bearing, in cases where the specific load capacity between the two bearing types is the same.

- An assessment on off-design operation suggests that groove geometries optimized for low compressibility numbers negatively impact the load capacity at higher values (i.e. higher rotor speed and smaller clearance). However, a design optimized for high compressibility numbers still present a significant gain at lower compressibility numbers compared to plain gas foil thrust bearing.

- The presence of grooves negatively impacts the ultimate load capacity of the thrust bearings compared to the plain GFTB.

It follows that the addition of spiral grooves on the GFTB's top foil can be an interesting solution to improve the load capacity and/or relieve the thermal management of plain gas foil thrust bearings. Due to the simplicity of the added manufacturing step, the proposed bearing layout is applicable to both new and commissioned bearings (retrofit).

Acknowledgment

The authors acknowledge the co-funding by the Swiss National Science Foundation, grant PYAPP2_154278/1.

Reference

[1] H. Heshmat, J. A. Walowit, O. Pinkus, Analysis of Gas Lubricated Compliant Thrust Bearings, Journal of Lubrication Technology 105 (4) (1983) 638–646. doi:10.1115/1.3254696.

[2] T. M. Conboy, Real-Gas Effects in Foil Thrust Bearings Operating in the Turbulent Regime, Journal of Tribology 135 (3) (2013) 031703–031703–12. doi:10.1115/1.4024048.

[3] L. San Andrés, K. Ryu, P. Diemer, Prediction of Gas Thrust Foil Bearing Performance for Oil-Free Automotive Turbochargers, Journal of Engineering for Gas Turbines and Power 137 (3) (2014) 032502–032502–10. doi:10.1115/1.4028389.

[4] T. H. Kim, M. Park, T. W. Lee, Design Optimization of Gas Foil Thrust Bearings for Maximum Load Capacity1, Journal of Tribology 139 (3) (2017) 031705–031705–11. doi:10.1115/1.4034616.

[5] K. Ryu, L. San Andrés, On the Failure of a Gas Foil Bearing: High Temperature Operation Without Cooling Flow, Journal of Engineering for Gas Turbines and Power 135 (11) (2013) 112506–112506–10. doi:10.1115/1.4025079.

[6] S. H. Prasad, D. Kim, Scaling Laws for Radial Clearance and Support Structure Stiffness of Radial Foil Bearings, Journal of Engineering for Gas Turbines and Power 139 (4) (2016) 042502. doi:10.1115/1.4034648.

[7] C. DellaCorte, R. J. Bruckner, Remaining Technical Challenges and Future Plans for Oil-Free Turbomachinery, Journal of Engineering for Gas Turbines and Power 133 (4) (2011) 042502. doi:10.1115/1.4002271.

[8] A. Lehn, Air foil thrust bearings: A thermo-elasto-hydrodynamic analysis, Ph.D. thesis, Technische Universität, Darmstadt (2017).

[9] D. Lee, D. Kim, Design and Performance Prediction of Hybrid Air Foil Thrust Bearings, Journal of Engineering for Gas Turbines and Power 133 (4) (2010) 042501–042501–13. doi:10.1115/1.4002249.

[10] H. Heshmat, H. M. Chen, I. Walton, J. F., On the Performance of Hybrid Foil-Magnetic Bearings, Journal of Engineering for Gas Turbines and Power 122 (1) (1999) 73–81. doi:10.1115/1.483178.

[11] S. B. Malanoski, C. H. T. Pan, The Static and Dynamic Characteristics of the Spiral-Grooved Thrust Bearing, Journal of Basic Engineering 87 (3) (1965) 547–555. doi:10.1115/1.3650603.

[12] H. Hashimoto, M. Ochiai, Optimization of Groove Geometry for Thrust Air Bearing to Maximize Bearing Stiffness, Journal of Tribology 130 (3) (2008) 031101–031101–11. doi:10.1115/1.2913546.

[13] J. Schiffmann, Enhanced Groove Geometry for Herringbone Grooved Journal Bearings, Journal of Engineering for Gas Turbines and Power 135 (10) (2013) 102501. doi:10.1115/1.4025035.

[14] L. Licht, W. J. Anderson, S. W. Doroff, Design and Performance of Compliant Thrust Bearings With Spiral-Groove Membranes on Resilient Supports, Journal of Lubrication Technology 103 (3) (1981) 373–384. doi:10.1115/1.3251681.

[15] N. Zirkelback, L. San Andrés, Effect of Frequency Excitation on Force Coefficients of Spiral Groove Gas Seals, Journal of Tribology 121 (4) (1999) 853–861. doi:10.1115/1.2834145.

[16] J. Schiffmann, Integrated design, optimization and experimental investigation of a direct driven turbocompressor for domestic heat pumps, Ph.D. thesis, École Polytechnique Fédérale de Lausanne (2008). doi:10.5075/epfl-thesis-4126.

[17] E. Guenat, J. Schiffmann, Real-gas effects on aerodynamic bearings, Tribology International 120 (2018) 358–368. doi:10.1016/j.triboint.2018.01.008.

[18] G. B. Leyland, Multi-objective optimisation applied to industrial energy problems, Ph.D. thesis, École Polytechnique Fédérale de Lausanne (2002). doi:10.5075/epfl-thesis-2572.

[19] V. N. Constantinescu, V. Castelli, On the Local Compressibility Effect in Spiral-Groove Bearings, Journal of Lubrication Technology 91 (1) (1969) 79–86. doi:10.1115/1.3554902.

[20] T. H. Kim, L. San Andrés, Limits for high-speed operation of gas foil bearings, Journal of tribology 128 (3) (2006) 670–673. doi:10.1115/1.2197851.

AppendixA. NGT

The terms composing equation 1 are developed here.

$$
\begin{aligned}
\bar{h}_r =& \frac{h_r}{h_0} = \frac{h_r}{h_r(\theta_R < \theta < \theta_B)} && \text{(A.1)}\\
\bar{h}_g =& \frac{h_g}{h_0} && \text{(A.2)}\\
\bar{\delta} =& \frac{h_g - h_r}{h_0} && \text{(A.3)}\\
g_1 =& \bar{h}_g^3 \bar{h}_r^3 && \text{(A.4)}\\
g_2 =& (\bar{h}_g^3 - \bar{h}_r^3)^2 \alpha(1-\alpha) && \text{(A.5)}\\
g_3 =& (1-\alpha)\bar{h}_g^3 + \alpha \bar{h}_r^3 && \text{(A.6)}\\
c_s =& \frac{6\mu\omega R^2}{p_a h_0^2} \alpha(1-\alpha)\bar{\delta}\sin\hat{\beta} && \text{(A.7)}\\
f_1 =& \frac{g_1 + g_2 \sin^2\hat{\beta}}{g_3} && \text{(A.8)}\\
f_2 =& \frac{g_2 \sin\hat{\beta}\cos\hat{\beta}}{g_3} && \text{(A.9)}\\
f_3 =& \frac{g_1 + g_2 \cos^2\hat{\beta}}{g_3} && \text{(A.10)}\\
f_4 =& \frac{\bar{h}_g^3 - \bar{h}_r^3}{g_3} && \text{(A.11)}\\
f_5 =& \alpha \bar{h}_g + (1-\alpha)\bar{h}_r && \text{(A.12)}
\end{aligned}
$$